Electromagnetically induced gratings in a degenerate open two-level system

G. C. Cardoso and J. W. R. Tabosa*
Departamento de Física, Universidade Federal de Pernambuco, 50670-901 Recife-PE, Brazil
(Received 24 October 2001; published 4 February 2002)

We have experimentally investigated laser diffraction on electromagnetically induced gratings in a degenerate open two-level system. The experiment employs the standard backward four-wave mixing configuration and the open $6S_{1/2}(F=4)\rightarrow 6P_{3/2}(F'=4)$ transition of cold cesium atoms. Population and coherence gratings are accessed for different relative polarizations of the incident laser beams. Natural and subnatural linewidths are observed depending on which frequency of the incident beams is scanned and reveal the effect of the atomic motion on the diffraction spectra. A simple theoretical model using a three-level Λ system is in reasonable agreement with the observed results and allowed us to make a close connection with the phenomenon of electromagnetically induced transparency.

DOI: 10.1103/PhysRevA.65.033803 PACS number(s): 42.50.Gy, 32.80.Pj, 42.65.Hw

I. INTRODUCTION

Electromagnetically induced transparency (EIT) [1] is a quantum interference phenomenon that can make a normally opaque transition completely transparent to a probe beam due to the coupling of a coherent pump field to a linked transition. This process can be described as a two-photon Raman transition and is enhanced when the two fields involved are perfectly coherent. Several applications have already been devised for EIT such as slow and ''frozen'' light [2], extremely sensitive magnetometers [3], sub-Doppler laser cooling [4], two-photon lasers [5], and squeezed light and studies on atomic coherence control [6]. The EIT phenomenon lies on the existence of coherent population trapping (CPT) and on the creation of dark states, that are atomic ground-states superpositions, which are not coupled to the excited state by the incident laser fields. Recent investigation on this effect has been performed using either hot [7] and cold [8,9] atomic vapors as well as solids [10]. The creation of such a coherent superposition of atomic states is associated with the induction of a coherence grating that can be used to Bragg diffract a third laser beam. Under appropriate conditions as regarding to which frequency of the incident laser beams is scanned, the diffracted signal can reveal the signature of the CPT and EIT phenomena.

Successful experimental observation of laser diffraction on a purely coherence grating was reported in hot sodium vapor by Hemmer *et al.* [11]. They used a phase conjugation four-wave mixing (PC-FWM) configuration and observed a very high efficiency for the PC-FWM process enhanced by the presence of CPT. On the other hand, a dark state grating can also be created when the pump beam used in the conventional EIT process is spatially modulated, giving rise to a spatially modulated EIT that can also Bragg diffract another incident beam. This effect has been theoretically proposed by Yuan Ling *et al.* [12] and recently observed by Mitsunaga and Imoto [13] using a forward FWM configuration in cold sodium atoms. According to Refs. [12] and [13], from now on these two types of coherence gratings and also the well-known case of induced population grating will be named generally as electromagnetically induced gratings (EIG). The observation of EIG spectra presents the advantage of being a background-free signal as opposite to the conventional observation of EIT.

Although most of the experiments realized on EIT employs the two hyperfine ground states of alkaline atoms, recent experiments have demonstrated this effect using the Zeeman sublevels of a degenerate two-level system (DTLS) [8,14,15]. In particular, for a transition between ground and excited levels with angular momentum equal to F_g and F_e, respectively, it has been shown that EIT is only present when $F_e \leqslant F_g$, otherwise one should observe electromagnetically induced absorption [14]. In a recent paper Wang *et al.* [16], reported the observation of forward FWM using the Zeeman sublevels of the Doppler-broadened open $F_g=2\rightarrow F_e=1$ transition in a hot rubidium vapor and showed that the FWM emission is strongly enhanced in the presence of CPT. The signature of EIT is usually associated with the observation of very narrow subnatural resonances, whose linewidths are determined by the ground-state lifetime. For the case of DTLS, depending on the relative polarization of the FWM beams, population and coherence gratings can be induced simultaneously and both types of gratings may lead to the observation of narrow resonances. It is worth mentioning that early experimental studies on the observation of narrow resonances in nearly degenerate FWM were performed by Lam *et al.* [17] using linearly polarized light and the cyclic transition ($F_g=2\rightarrow F_e=3$) of hot sodium vapor. Later on Berman *et al.* [18] also considered this subject for open and closed degenerate two-level transitions and described the radiative-induced narrow resonances as being due to the nonconservation of population, alignment or orientation. Also, an early theoretical study [19] predicted the observation of narrow resonances in degenerate PC-FWM for a pure Λ system and called the attention for saturation effects as a result of the interplay between Zeeman coherence and modulated population mechanisms.

This paper is concerned with the diffraction of a laser beam on EIG, induced on a sample of cold cesium atoms, using the nearly degenerate PC-FWM configuration. Linearly polarized light is employed to create the induced grat-

*Email address: tabosa@df.ufpe.br

ings in the degenerate open two-level system $6S_{1/2}(F=4) \rightarrow 6P_{3/2}(F'=4)$. Depending on the relative polarizations, and on which frequency of the incident beams is scanned, different types of gratings can be evidenced, leading to the observation of natural and subnatural linewidth signals. A simple theoretical model using the density-matrix formalism in a three-level system accounts reasonably for the main observed results, and in particular, for the effect of the atomic motion on the different induced gratings. The paper is organized as follows. In Sec. II, we describe qualitatively the different types of EIG on a DTLS associated with different relative polarizations of the incident beams. In Sec. III, we describe the experiment and present the observed results. Section IV is dedicated to the interpretation of the experimental observations in view of a simple-density matrix calculation. Finally, our conclusions come in Sec. V.

II. COHERENCE AND POPULATION GRATINGS

In a pure two-level system the resonant PC-FWM signal can be understood as a diffraction of the pump beams on population gratings induced by the other incident beams [20]. If this two-level system is open, narrow resonances associated with the ground-state population relaxation rate may appear when this rate is smaller than one of the excited state [21]. Such a behavior can be found, for example, in a DTLS with arbitrary but equal angular momenta, F_g and F_e, excited by a forward beam (F) and a backward beam (B), having the same frequency $\omega_F=\omega_B=\omega$ and by a probe beam (P) with frequency $\omega_P=\omega+\delta$, in the standard PC-FWM configuration shown in Fig. 1(a). When all the beams have the same linear parallel polarization, the system behaves as a set of open two-level systems coupled by spontaneous emission, as depicted in Fig. 1(b), where we define the quantization direction as being parallel to the common laser beams polarization. In this case, the PC-FWM signal originates from diffraction on induced purely populational gratings and the narrow resonance around $\delta=0$ is a manifestation of optical pumping induced nonconservation of multipolar terms of the atomic density matrix [18]. On the other hand, when the FWM beams have different linear polarizations, different types of gratings are induced in the system. For example, if the beams have the same frequency as above, but the polarization of F is perpendicular to that of B and P beams, as depicted in Fig. 1(c), the signal originates from two distinct induced gratings: (i) diffraction of beam B in the coherence grating induced by beams F and P, and (ii) diffraction of the F beam in a population grating induced by the B and P beams. In this case, when we scan δ, both gratings lead to the observation of narrow resonance around $\delta=0$. Although we cannot separate these two contributions for the generated signal for a sample of immobile atoms, for such an open system even the narrow velocity distribution of cold atoms in a magneto-optical trap can play a very important role for the washout of induced gratings. This happens because the grating dynamics is determined by the small ground-state relaxation rate, which can be comparable to the inverse of the time it takes for the atom to move one grating period. It is worth mentioning that for a closed two-level system in the range of velocities of laser-cooled atoms, the effect of velocity is completely negligible since the induced gratings will decay with the spontaneous emission lifetime, leading to a diffracted signal with natural linewidth [22].

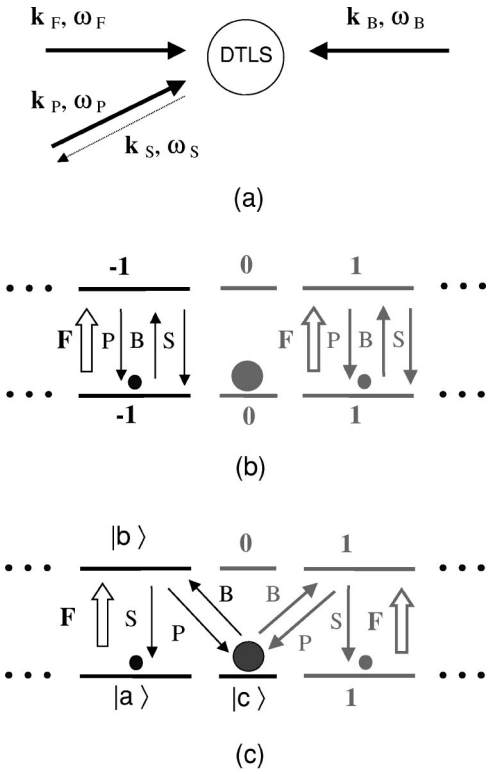

FIG. 1. (a) Backward PC-FWM beam configuration. $\mathbf{k}_\mu$ and ω_μ ($\mu=F,P,B$) are the corresponding wave vectors and frequencies of the FWM beams. (b) Zeeman sublevels of a DTLS associated with a $F_g \rightarrow F_e$ transition, with $F_g=F_e>1$. The dots indicate that the other Zeeman sublevels are not shown. In this case the PC-FWM fields are supposed to be all polarized parallel to the quantization axis and the arrows represent the interaction between the fields and the DTLS. The dark circles indicate the Zeeman-level population. (c) Idem, for beams P and B polarized perpendicularly to the atomic quantization axis, defined by the F beam polarization direction.

III. EXPERIMENTAL OBSERVATIONS IN COLD CESIUM

The experiment was performed in a sample of cold cesium atoms obtained from a magneto-optical trap (MOT) and employed the conventional backward PC-FWM configuration as shown schematically in Fig. 2(a). The angle between the forward (F) and the probe (P) beams is approximately 40 mrad. The experimental setup is a slight modification of the one previously described in Ref. [23], so here we will describe it very briefly. The light beams for the MOT and for the nearly degenerate FWM process are provided by the same Ti:Sapphire laser that is red detuned by about 11 MHz below the resonance frequency of the cesium closed transition $6S_{1/2}(F=4) \rightarrow 6P_{3/2}(F'=5)$. In the experiment, the frequency of only one of the three incident beams (F, P, or B) is scanned at a time. The fixed frequency beams are obtained

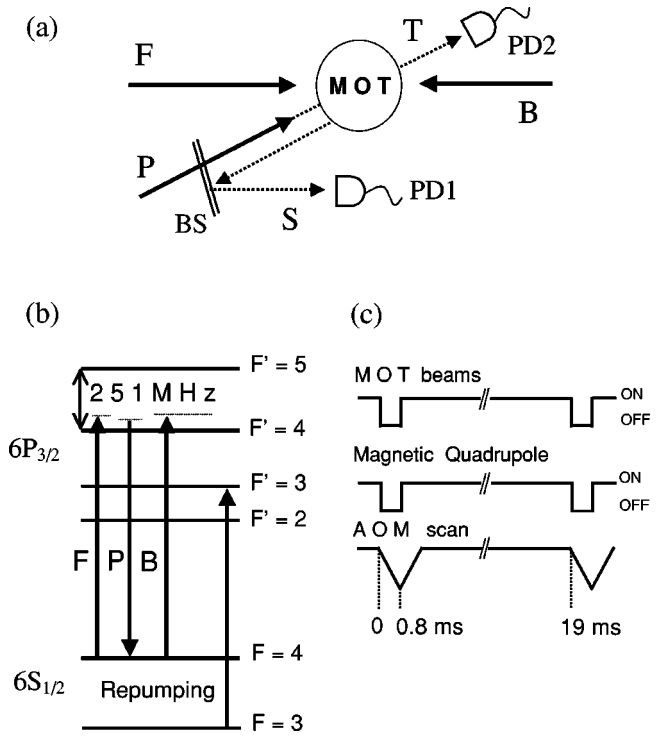

FIG. 2. (a) Simplified experimental setup. Photodiode PD1 measures the EIG signal while photodiode PD2 measures the probe transmission signal. (b) Hyperfine levels of the cesium $D2$ line, indicating the frequencies of the F, P, and B beams as well as that of the repumping beam. Trapping beams are omitted. (c) Temporal beam switching and frequency scan scheme.

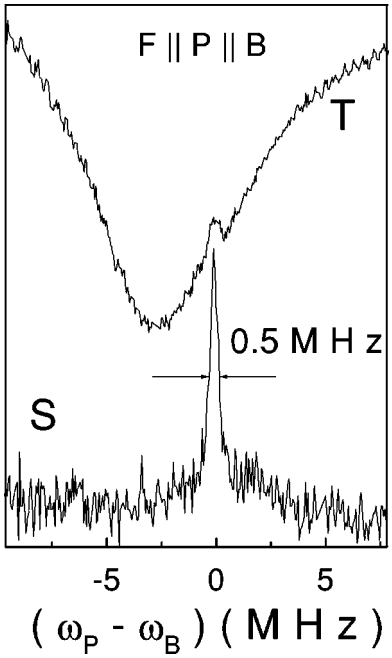

FIG. 3. Probe beam transmission (T) and EIG signal (S) spectra for the case where all the FWM beams have parallel linear polarizations. The maximum of absorption in the figure is around 50%. There is a slight reduction in the contrast of the EIT signal due to fluctuation in the absorption level during the signal averaging.

from the Ti:Sapphire laser by shifting its frequency down by approximately 240 MHz through the use of an acousto-optic modulator (AOM) which brings this frequency to near resonance with the open cesium transition $6S_{1/2}(F=4) \rightarrow 6P_{3/2}(F'=4)$, according to the cesium level scheme shown in Fig. 2(b). A second AOM whose radio frequency (~ 120 MHz) is controlled by the voltage ramp depicted in Fig. 2(c) shifts down the Ti:Sapphire frequency in double passage, with the aid of a spherical mirror, producing a beam whose frequency can be scanned around the resonance frequency of the $6S_{1/2}(F=4) \rightarrow 6P_{3/2}(F'=4)$ transition. The generated phase conjugate beam is reflected out of a 50/50 beam splitter and detected by the photodiode PD1 shown in Fig. 2(a). The probe transmission is detected by the photodiode PD2. Both signals are averaged by a digital oscilloscope for 64 successive scans. The relative polarization between the pump and the probe fields is controlled by wave plates. The spectra were recorded within a ~ 0.8 ms time interval during which the trapping beams were blocked by a mechanical chopper (with a transmission duty cycle of $\sim 95\%$) and the quadrupole magnetic field was turned off. The number of cold atoms was estimated by measuring the absorption of a probe beam and was of order of 10^7. The $1/e$ lifetime of the MOT after switching off the trapping beams was measured to be of the order of 2 ms. To avoid optical pumping to the $6S_{1/2}(F=3)$ level, the repumping beam was kept on during the measurements. In fact, all the measured signals are very sensitive to the repumping efficiency. There was no compensation for the earth's or other environmental magnetic fields. Nevertheless, the signal is not very sensitive to small magnetic fields as we have checked by letting the anti-Helmholtz fields on in some measurements with no appreciable change in the observed signals.

In Fig. 3, we show a typical spectrum for the PC-FWM signal (S) and for the probe beam transmission (T), corresponding to the case where all the beams have the same linear parallel polarization. This spectrum is measured as a function of the probe beam frequency offset relative to the common frequency of the F and B beams, which are kept fixed and detuned by about 3 MHz above the atomic resonance frequency. In this spectrum, the beams intensities used were $I_P \simeq 30$ μW/cm^2 and $I_F = I_B \simeq 0.4$ mW/cm^2. As we have discussed, for this polarization configuration the narrow PC-FWM spectrum as well as the narrow feature present in the probe transmission spectrum are related to the dynamics of the ground-state population of open two-level systems. The maximum observed probe reflectivity, of the order of 0.1%, was measured for this configuration. In Fig. 4, we present the PC-FWM spectra and the corresponding probe transmission spectra for the case where the F and P beams have linear parallel polarizations perpendicular to that of the B beam. The spectra presented in Figs. 4(a) and 4(b) are measured, respectively, as a function of the frequency of the P and F beams, while keeping the frequencies of the other two incident beams equal and detuned by about 3 MHz above the atomic resonance. In both cases, the zero of the frequency scale is taken relative to the frequency that is kept fixed. The beams intensities in Fig. 4(a) are the same as specified in Fig. 3, and in Fig. 4(b) the beams intensities used

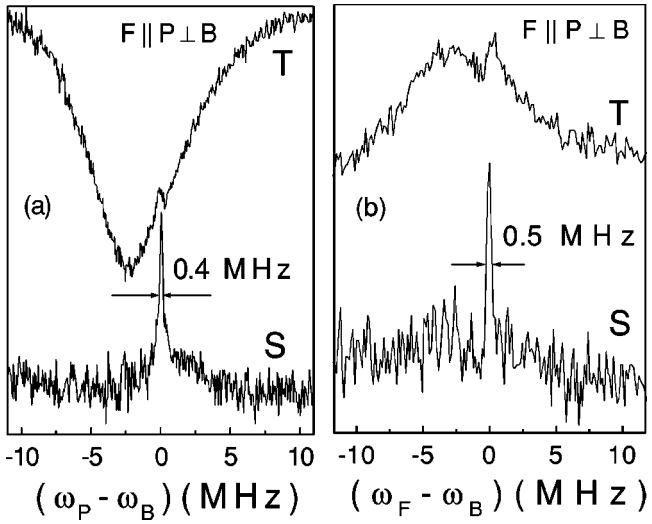

FIG. 4. Probe beam transmission (T) and EIG signal (S) spectra when all beams polarizations are linearly polarized but the polarization of the B beam is perpendicular to the common polarization of the F and P beams. (a) ω_P is scanned with $\omega_F=\omega_B$ fixed. (B) ω_F is scanned with $\omega_P=\omega_B$ fixed. The fixed frequency beams detuning is around 3 MHz above the atomic resonance.

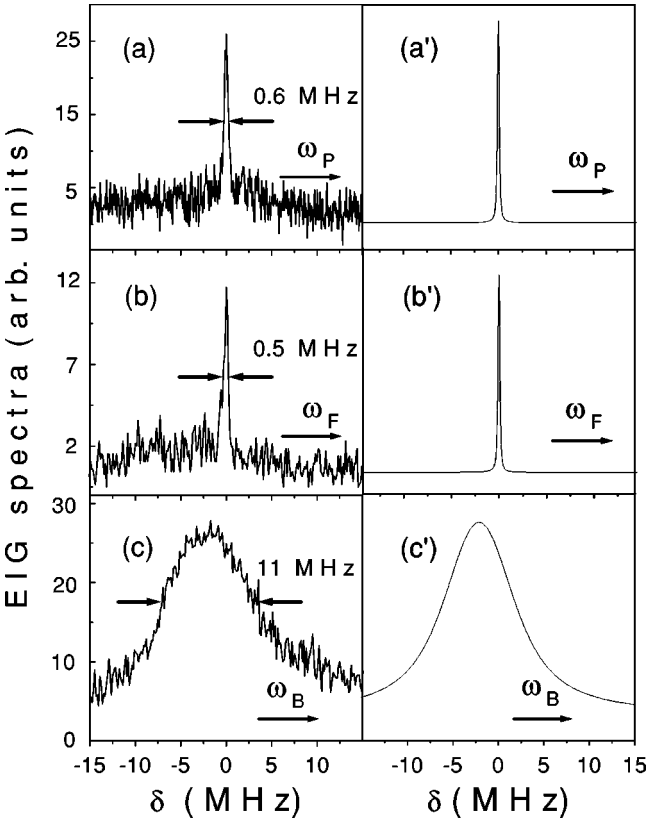

FIG. 5. (a)–(c) EIG signals for linear polarizations of the FWM beams, with the polarization of the F beam perpendicular to the common polarization of the B and P beams. (a′)–(c′) are calculated spectra using the theoretical model described in the text and averaging on velocities. In (a),(a′) ω_P is scanned with $\omega_F=\omega_B$ fixed, and $\delta=\omega_P-\omega_F$; in (b),(b′) ω_F is scanned with $\omega_P=\omega_B$ fixed, and $\delta=\omega_F-\omega_P$; in (c),(c′) ω_B is scanned with $\omega_P=\omega_F$ fixed, and $\delta=\omega_B-\omega_F$. The fixed frequency beams detuning is around 3 MHz above the atomic resonance.

were $I_P\simeq 0.2$ mW/cm^2, $I_F\simeq 0.2$ mW/cm^2, and $I_B\simeq 30$ μW/cm^2. The narrow features present in Fig. 4 are clearly associated with the usual EIT phenomenon because in this case the relative beams polarization can create a coherent superposition of ground-state Zeeman sublevels. In Fig. 4(b) the inversion of the broad resonance in the probe transmission spectrum, observed when the frequency of the F beam is scanned, is due to optical depumping of the $6S_{1/2}(F=4)$ population induced by the strong F beam. Notice that in both cases the broad absorption peak is centered around the atomic resonance frequency. While the contrast of the EIT peaks appears slightly diminished after signal averaging due to fluctuations in the absorption level, the EIG signals are less sensitive to this effect since they correspond to background-free signals. The observed fluctuation in the absorption level is related to fluctuation in the number of trapped atoms and is mainly due to the small drift in the repumping laser frequency that was not locked. Owing to the absorption of the pump beam, these fluctuations can affect differently the EIT peak and the main absorption line.

Another interesting polarization configuration we have analyzed corresponds to the case where the polarization of the F beam is perpendicular to the common linear polarization of the P and B beams. We have chosen this configuration to compare the observed spectra with a simple theoretical model as we will describe in the following section. The PC-FWM spectra corresponding to this relative beams polarization are presented in Figs. 5(a)–5(c), for the cases where we scan the frequency of the P, F, and B beams, respectively. As observed, when one scan the frequency of the B beam the diffracted signal does not present any subnatural linewidth feature. This behavior was observed for all the relative polarizations configurations studied in this paper. The beams intensities corresponding to Fig. 5(a) are the same as those used in Fig. 3, while the beams intensities used in Figs. 5(b) and 5(c) are the same as in Fig. 4(b).

IV. MODEL AND DISCUSSION

The aim of this section is to present the simplest theoretical model to account for the main characteristics of the observed experimental results. As we have mentioned, when the polarizations of all the beams are linear and parallel, the system can be conveniently described as a set of independent open two-level systems. However, for linearly polarized beams, with the F beam polarization perpendicular to that of the P and B beams, the DTLS presents a prominent character of a Λ system, as suggested in Fig. 1(c). An important feature of the $F=4\rightarrow F'=4$ transition is that the $m=0\rightarrow m'=0$ Clebsch-Gordan coefficient is zero, leading to a population trapping in the $m=0$ Zeeman sublevel [Fig. 1(c)]. We account for the escape of atoms from the interaction region by an effective ground-state relaxation rate γ. The effect of the repumping beam and the arrival of fresh atoms with equiprobable chance to be in any Zeeman sublevel permit the creation of a nonzero Zeeman population in the $m\neq 0$ sub-

levels. With these considerations one sees that for high intensity of the F beam, whose polarization direction is taken as defining the quantization axis, the DTLS will behave as three-level Λ systems, where most of the population is in the ground-state $m=0$. We will therefore model our system as the $|a\rangle$-$|b\rangle$-$|c\rangle$ Λ system specified in Fig. 1(c), interacting with the three incident FWM beams having the linear polarization specified above. The strong F beam with frequency ω_F, is coupled to the transition $|a\rangle$-$|b\rangle$ while the beams P and B, with frequencies ω_P and ω_B, respectively, are coupled to the transition $|b\rangle$-$|c\rangle$. In the perturbative density-matrix calculation performed below, the F beam is supposed to be strong and will be considered in all orders of perturbation, while the other beams are weak and will be considered only in first order [24]. The Liouville equation describing the system is

$$\dot{\rho}=\frac{1}{i\hbar}[H,\rho]-\left.\frac{d\rho}{dt}\right|_{relax}, \tag{4.1}$$

where $\dot{\rho}=(\partial/\partial t+\mathbf{v}\cdot\boldsymbol{\nabla})\rho$, with $\vec{v}$ being the atomic velocity, is the hydrodynamic derivative and $d\rho/dt|_{relax}$ accounts for the phenomenological relaxation terms of the density-matrix elements. We assume that the relaxation rate is γ for the populations ρ_{aa} and ρ_{cc}, and 2Γ for ρ_{bb}, with $\gamma\ll\Gamma$. For the sake of simplicity, the Λ system is supposed to be open only in the ground-states. For the relaxation rates of the coherence terms, we therefore have γ for the ρ_{ac} coherence and Γ for the coherences ρ_{ab} and ρ_{bc}, since $\gamma\ll\Gamma$. The Hamiltonian of the system interacting with the three incident fields is given by

$$H=H_o+V_F+V_P+V_B, \tag{4.2}$$

$$H_o=\omega_a|a\rangle\langle a|+\omega_b|b\rangle\langle b|+\omega_c|c\rangle\langle c|, \tag{4.3}$$

$$V_F=-\Omega_F\exp[i(\omega_F t-\mathbf{k_F}\cdot\mathbf{r}]|a\rangle\langle b|+\text{H.c.}, \tag{4.4}$$

$$V_P=-\Omega_P^*\exp[-i(\omega_P t-\mathbf{k_P}\cdot\mathbf{r}]|b\rangle\langle c|, \tag{4.5}$$

$$V_B=-\Omega_B\exp[i(\omega_B t-\mathbf{k_B}\cdot\mathbf{r}]|c\rangle\langle b|, \tag{4.6}$$

where $\Omega_F=\mu_{ab}E_F/2\hbar$, $\Omega_P=\mu_{bc}E_P/2\hbar$, and $\Omega_B=\mu_{bc}E_B/2\hbar$ are the corresponding Rabi frequencies, and the remaining symbols use standard notation. In the Hamiltonian above, we have omitted the terms that would not contribute to the signal in the direction of the PC-FWM emission.

The perturbative calculation developed below consists in expanding the density-matrix element in powers of the incident P and B electrical fields and in solving the Liouville equation for each pertubative order. We denote by $\rho^{(\mathbf{F},P,B)}$ the density-matrix element in all orders in the F field and in first order in the P and B fields. As we have discussed above, in our approximation, the zero-order solution in P and B, i.e., $\rho^{(\mathbf{F},0,0)}$, is taken to have only one nonzero element, namely, $\rho_{cc}^{(\mathbf{F},0,0)}=1$. The expression for the perturbation order of interest is given by

$$\dot{\rho}^{(\mathbf{F},P,B)}=\frac{1}{i\hbar}[H_o,\rho^{(\mathbf{F},P,B)}]+\frac{1}{i\hbar}[V_F,\rho^{(\mathbf{F},P,B)}]+\frac{1}{i\hbar}[V_B,\rho^{(\mathbf{F},P,0)}]+\frac{1}{i\hbar}[V_P,\rho^{(\mathbf{F},0,B)}]-\left.\frac{d\rho}{dt}\right|_{relax}. \tag{4.7}$$

In Eq. (4.7), the second term on the right-hand side is associated with a population grating induced by the P and B beams that diffracts the F beam along the PC-FWM emission direction, while the third term describes the coherence grating induced by the F and P beams that diffracts the B beam along that same direction. We can therefore calculate the induced coherence in the transition $|a\rangle-|b\rangle$, which is responsible for the PC-FWM emission. Neglecting propagation effects, the PC-FWM signal is proportional to the square modulus of

$$\rho_{ab}^{(\mathbf{F},P,B)}=\rho_{ab\text{-}coh}^{(\mathbf{F},P,B)}+\rho_{ab\text{-}pop}^{(\mathbf{F},P,B)}, \tag{4.8}$$

where

$$\rho_{ab\text{-}coh}^{(\mathbf{F},P,B)}=\frac{i\Omega_F\Omega_P^*\Omega_B\exp\{\mathbf{i}[(\omega_F-\omega_P+\omega_B)t-(\mathbf{k_F}-\mathbf{k_P}+\mathbf{k_B})\cdot\mathbf{r}]\}}{8\{[i(\omega_F-\omega_P)-i(\mathbf{k_F}-\mathbf{k_P})\cdot\mathbf{v}+\gamma][\mathbf{i}(\omega_{\mathbf{bc}}-\omega_{\mathbf{p}})+\mathbf{i}\mathbf{k_P}\cdot\mathbf{v}+\mathbf{\Gamma}]+|\mathbf{\Omega_F}|^2\}}\times\frac{1}{[i(\omega_F-\omega_P+\omega_B-\omega_{ba})+i\mathbf{k_P}\cdot\mathbf{v}+\Gamma+p|\Omega_F|^2]}, \tag{4.9}$$

$$\rho_{ab\text{-}pop}^{(\mathbf{F},P,B)}=\rho_{ab\text{-}coh}^{(\mathbf{F},P,B)}\left(\frac{[i(\omega_F-\omega_P)+i(\mathbf{k_F}-\mathbf{k_P})\cdot\mathbf{v}+\gamma]}{[i(\omega_B-\omega_P)+i(\mathbf{k_B}-\mathbf{k_P})\cdot\mathbf{v}+\gamma]}\right)\left(\frac{[i(\omega_B-\omega_P)+i(\mathbf{k_B}-\mathbf{k_P})\cdot\mathbf{v}+\gamma-\mathbf{\Gamma}]}{[i(\omega_B-\omega_P)+i(\mathbf{k_B}-\mathbf{k_P})\cdot\mathbf{v}+2\mathbf{\Gamma}]}\right), \tag{4.10}$$

with p given by

$$p=\frac{2i(\omega_B-\omega_P)-2i(\mathbf{k_B}-\mathbf{k_P})\cdot\mathbf{v}+\mathbf{\Gamma}+\gamma}{[i(\omega_B-\omega_P)-i(\mathbf{k_B}-\mathbf{k_P})\cdot\mathbf{v}+\gamma][\mathbf{i}(\omega_{\mathbf{B}}-\omega_{\mathbf{P}})-\mathbf{i}(\mathbf{k_B}-\mathbf{k_P})\cdot\mathbf{v}+2\mathbf{\Gamma}]}. \tag{4.11}$$

The terms $\rho_{ab\text{-}coh}^{(\mathbf{F},P,B)}$ and $\rho_{ab\text{-}pop}^{(\mathbf{F},P,B)}$ represent the coherences induced on the transition $|a\rangle$-$|b\rangle$ and describe the contribution for the generated signal associated, respectively, with the diffraction on the coherence and on the population gratings mentioned above. The PC-FWM signal line shapes predicted by Eq. (4.8) present natural and subnatural linewidth features depending on which frequency of the FWM beams is scanned and, for a sample of completely immobile atoms, both the coherence and population terms contribute to the generated signal. The contribution of the different EIG for the generated signal is strongly dependent on the atomic motion, even in the limit of very small velocities associated with laser-cooled atoms [25]. In addition, each grating is affected differently by the atomic motion since for small angle between the *F* and *P* beams, the corresponding coherence grating has a spatial period much larger than the population grating that is associated with the *B* and *P* beams.

In the low saturation regime, where $\Omega_F \ll \Gamma$, when we scan the frequency ω_F while keeping the frequencies ω_P and ω_B equal and close to the atomic resonance, the coherence term will contribute with a narrow peak of width γ, centered around $\delta_F = \omega_F - \omega_P = 0$ that is not affected by the atomic motion. However, the contribution arising from the population term consists essentially of a broad peak with width of the order of 2Γ centered around the atomic resonance with a dip of width γ around $\delta_F = 0$. This contribution is velocity dependent and decreases significantly when the velocity average is performed. Differently, for the case where we scan the frequency ω_B again keeping the others beams frequencies fixed and close to the atomic resonance, it is the coherence term that presents a broad peak of width 2Γ, centered around the atomic resonance with a narrow dip of width γ around $\delta_B = \omega_B - \omega_P = 0$, while the population term contributes with a narrow peak of width γ, around $\delta_B = 0$. In this case, the velocity average washes out only the narrow features present in both the coherence and population terms. Finally, when the frequency ω_P is scanned, both terms give rise only to narrow contributions of width γ around the common laser frequency, with the contribution originating from the population term being the one more affected by the velocity average. We can summarize the above results by observing that in all the three cases analyzed, the effect of the atomic velocity is appreciable only for the signal originating from diffraction in the grating associated with the *P* and *B* beams, which has a much smaller spatial period. We also notice that the subnatural linewidth signals are observed only for PC-FWM associated with diffraction on a nonstationary EIG.

The calculated spectra corresponding to the observed spectra presented in Figs. 5(a)–5(c), and associated with the three cases discussed above, are shown in Figs. 5(a′)–5(c′). The calculated spectra were velocity averaged using a Maxwell-Boltzmann velocity distribution with a mean velocity of $u = 0.35$ m/s, which corresponds to trap temperatures of the order of 1 mK, as measured for our MOT [26]. In the calculation we have used $\Omega_F = 0.3\Gamma$, in reasonable accordance with the average experimental values and $\gamma/\Gamma = 0.01$, with $2\Gamma = 5.23$ MHz. As we can see the calculated spectra reproduce reasonably well the observed results corresponding to different dynamics of the induced gratings.

V. CONCLUSIONS

We have experimentally investigated nearly degenerate PC-FWM in an open degenerate two-level system consisting of cold cesium atoms. The observed PC-FWM signal is interpreted as a diffraction process into different types of electromagnetically induced gratings and are strongly connected with the effect of EIT and CPT in the corresponding DTLS. We have also showed the important role played by the atomic motion even in the limit of very small velocities associated with laser-cooled atoms. This velocity dependence arises from the induction of gratings whose dynamics is determined by the ground-state relaxation rate. A simple theoretical model was developed and accounts reasonably for the main characteristic of the observed results. Through a precise determination of the relevant parameters this observed velocity dependence could provide another method to measure the temperature of the cold atomic sample.

ACKNOWLEDGMENTS

The authors acknowledge fruitful discussions with A. Lezama and D. Bloch. This work was supported by CNPq (PRONEX), CAPES, and FINEP (Brazilian agencies).

[1] S. E. Harris, Phys. Today, **50**(7), 36 (1997), and references therein.

[2] C. Liu, Z. Dutton, C.F. Behroozi, and L.V. Hau, Nature (London) **409**, 490 (2001); D.F. Phillips, A. Fleischhauer, A. Mair, R.L. Walsworth, and M.D. Lukin, Phys. Rev. Lett. **86**, 783 (2001).

[3] M.O. Scully and M. Fleischhauer, Phys. Rev. Lett. **69**, 1360 (1992); M. Stähler, S. Knappe, C. Affolderbach, W. Kemp, R. Wynands, Europhys. Lett. **53**, 323 (2001).

[4] C.F. Roos, D. Leibfried, A. Mundt, F. Schmidt-Kaler, J. Eschner, and R. Blatt, Phys. Rev. Lett. **85**, 5547 (2000).

[5] O. Pfister, W.J. Brown, M.D. Stenner, and D.J. Gauthier, Phys. Rev. Lett. **86**, 4512 (2001).

[6] B.S. Ham and P.R. Hemmer, Phys. Rev. Lett. **84**, 4080 (2000).

[7] Yufu Zhu, Shijun Wang, and Neil M. Mulchan, Phys. Rev. A **59**, 4005 (1999); Yong-qing Li and Min Xiao, Opt. Lett. **21**, 1064 (1996).

[8] A.V. Durrant, H.X. Chen, S.A. Hopkins, and J.A. Vaccaro, Opt. Commun. **151**, 136 (1998).

[9] M. Yan, E.G. Rickey and Y. Zhu, Opt. Lett. **26**, 548 (2001).

[10] B.S. Ham, M.S. Shahriar, and P.R. Hemmer, Opt. Lett. **22**, 1138 (1997).

[11] P.R. Hemmer, D.P. Katz, J. Donoghue, M. Cronin-Galomb, M.S. Shahriar, and P. Kumar, Opt. Lett. **20**, 982 (1995).

[12] Hong Yuan Ling, Yong-Qing Li, and Min Xiao, Phys. Rev. A **57**, 1338 (1998).

[13] Masaharu Mitsunaga and Nobuyuki Imoto, Phys. Rev. A **59**, 4773 (1999).
[14] A.M. Akulshin, S. Barreiro, and A. Lezama, Phys. Rev. A **57**, 2996 (1998).
[15] V. Milner and Y. Prior, Phys. Rev. Lett. **80**, 940 (1998).
[16] S. Wang, D.G. Ducreay, R. Pina, Min Yan, and Yifu Zhu, Phys. Rev. A **61**, 033805 (2000).
[17] J.F. Lam, D.G. Steel, and R.A. McFarlane, Phys. Rev. Lett. **56**, 1679 (1986).
[18] P.R. Berman, D.G. Steel, Galina Khitrova, and Jing Liu, Phys. Rev. A **38**, 252 (1988).
[19] C. Schmidt-Iglesias, Phys. Rev. A **46**, 7210 (1992).
[20] D.M. Bloom, P.F. Liao, and N.P. Economou, Opt. Lett. **2**, 58 (1978).
[21] D.G. Steel and J.T. Remillard, Phys. Rev. A **36**, 4330 (1987).
[22] M. Ducloy and D. Bloch, J. Phys. (France) Lett. **42**, 711 (1981).
[23] A. Lezama, G.C. Cardoso, and J.W.R. Tabosa, Phys. Rev. A **63**, 013805 (2000).
[24] M. Pinard, B. Kleinmann, G. Grynberg, D. Bloch, and M. Ducloy, J. Phys. (France) Lett. **46**, 149 (1985).
[25] G.C. Cardoso, V.R. de Carvalho, S.S. Vianna, and J.W.R. Tabosa, Phys. Rev. A **59**, 1408 (1999).
[26] J.W. Tabosa, A. Lezama, and G.C. Cardoso, Opt. Commun. **165**, 59 (1999).